Three-Dimensional Electromagnetic Modeling of Fiber-Core Effects on the Coupling Characteristics of Weakly Fused Tapered Fiber-Optic Couplers

Tzong-Lin Wu, *Member, IEEE*

***Abstract*—Based on the full-wave formulations, which combine the finite element method and the boundary element technique, and the step-like approximation method, a three-dimensional (3-D) electromagnetic modeling approach is proposed in this work to investigate the fiber-cores effects on the coupling characteristics of the weakly fused tapered couplers. We find the fiber cores have significant effects on the mode field patterns, coupling coefficients, and birefringence for the coupler with large normalized frequencies. The influence of the fiber cores on the coupling behavior for the real couplers, such as 3 dB power dividers, polarization beam splitters, and wavelength demultiplexing/multiplexing couplers, are also studied in 3-D view. It is found that the effects of fiber-cores in the weakly fused tapered couplers have to be considered for accurately modeling their coupling behavior, although the model with no-core assumption can predict the trend of the coupling characteristics for the real couplers.**

***Index Terms*—Electromagnetic modeling, fiber-cores effect, fiber-optic couplers, vectorial optical waveguide theory, weakly fused couplers.**

I. Introduction

FUSED fiber-optic couplers are made by fusing and then tapering two identical fibers The couplers consist of three regions: fiber-core, fiber-cladding, and the surrounding medium which is air unless some packaging material is used. Since the transverse dimension of the coupler in the tapering process is reduced and the cross-sectional area of the cores become very small, the presence of the fiber-cores is usually neglected in analyzing the coupling characteristics of the fused couplers. This paper investigates the fiber-core effects on the coupling behavior of the weakly fused tapered coupler based on three-dimensional (3-D) electromagnetic (EM) numerical modeling.

Accurate 3-D EM modeling of the performance of the couplers is quite important for designing the couplers with proper function and for understanding their coupling characteristics. Several works have been contributed to the 3-D EM modeling of the biconical tapered couplers [1]–[5]. A combination of effective index method (EIM) and step-like approximation method was employed to model the coupling behavior of the fused tapered couplers [2]–[4], such as polarization beam-splitter and wavelength-flattened couplers. The EIM, which approximates a two-dimensional dumbbell-shaped structure to an equivalent one-dimensional slab waveguide with fiber-core being concerned, is not able to accurately predict the polarization property of the coupler, especially in weakly fused conditions [6], [7]. A rigorous 3-D modeling approach, which combines the surface integral equation method (SIEM) [8] and the step-like approximation method, was recently proposed to treat the coupling phenomena of the polarization beam splitter with concerning the form birefringence effect [5]. In this approach, the fiber-core effects are neglected and the coupling characteristics of the homogeneous embedded waveguide with dumbbell-shaped cross section are rigorously solved by SIEM. However, fiber-cores are obviously seen in the weakly fused couplers by experimental measurement [9] and their effects on the coupling characteristics are theoretically shown significant by the EIM [10]. To rigorously find the fiber-core effects on the coupling characteristics of the couplers and improve the modeling accuracy for the weakly fused tapered couplers, a vectorial 3-D EM modeling approach with the fiber-cores being concerned is necessary.

Based on the full-wave vectorial formulations [11], which combines the finite-element method (FEM) and the boundary-element method (BEM), and the step-like approximation method, a 3-D EM modeling approach for the weakly fused tapered fiber-optic couplers with cores effect being concerned is proposed in this paper. Section II describes the theoretical bases for our 3-D EM modeling approach for the weakly fused couplers. In Section III, the fiber-core effects on the coupling characteristics and mode field patterns are investigated in two-dimensional (2-D) view. The influence of the cores effects on the coupling behaviors of the real couplers, such as power dividers, polarization beam-splitters and wavelength demultiplexing/multiplexing couplers, is investigated in Section IV by the proposed 3-D EM modeling approach. The conclusion is drawn in Section V.

II. 3-D EM Modeling Approach

Sketches of a weakly fused tapered coupler and its dumbbell-shaped cross section are shown in Fig. 1(a) and (b), respectively. Consider that an unpolarized light P_0, which is initially guided in the fiber-core, is launched into one of the input ports. In the tapered region the power is gradually guided between the fiber-cladding and the surrounding medium, and the

Manuscript received November 11, 1999; revised March 14, 2000. This work was supported by the National Science Council of the Republic of China under grant NSC88-2218-E-110-009.

The author is with the Department of Electrical Engineering, National Sun Yat-sen University, Kaohsiung, Taiwan 80424, R.O.C.

Publisher Item Identifier S 0733-8724(00)05762-5.

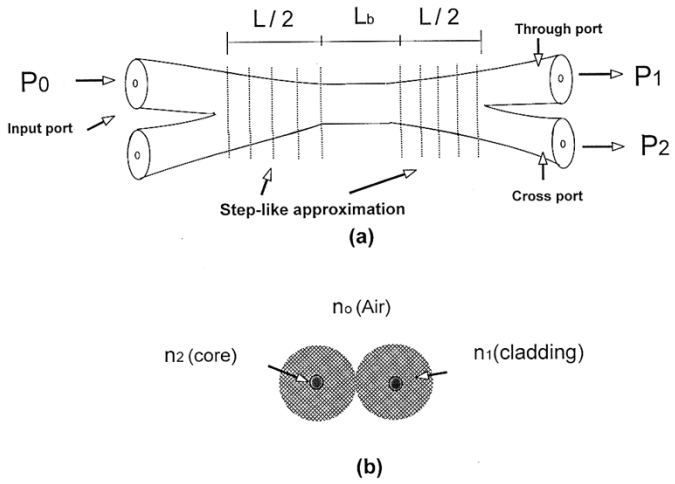

Fig. 1. (a) Sketch of a fused tapered fiber-optic coupler where L_b is the burned length and L is the drawn length. (b) The cross section of a realistic coupler in weakly fused condition.

four lowest order modes, which are symmetric (even) and antisymmetric (odd) modes of x polarization state and the corresponding modes of y polarization, are excited. The coupling mechanism of the coupler is the beating of the even and odd modes in the coupling region of the composite optical waveguide. If we assume that $P_0 = P_{0x} + P_{0y}$, the output powers at through port and crossport are then given by

$$P_1 = P_{1x} + P_{1y} = P_{0x}\cos^2\Delta\phi_x + P_{0y}\cos^2\Delta\phi_y \quad (1a)$$

$$P_2 = P_{2x} + P_{2y} = P_{0x}\sin^2\Delta\phi_x + P_{0y}\sin^2\Delta\phi_y \quad (1b)$$

respectively, where $\Delta\phi_x$ and $\Delta\phi_y$ denote the accumulated phase differences along the coupling region between the even and odd modes for the light with x and y polarization state, respectively. $\Delta\phi_x$ and $\Delta\phi_y$ can be calculated from

$$\Delta\phi_i = \int [(\beta_e^i - \beta_o^i)/2]\,dz = \int C_i\,dz$$

where $C_i = (\beta_e^i - \beta_o^i)/2$ is defined as the coupling coefficient of i (= x or y) polarization and β_e^i and β_o^i are propagation constants of the even and odd modes, respectively, for the their corresponding polarization. Therefore, precisely finding the propagation constants of those four lowest order normal modes at each point along the coupler is the key to accurately model the coupling characteristics of the couplers.

Fig. 2 gives a sketch of the dumbbell-shaped cross section of the weakly fused couplers with two identical fibers being just touching, where b and r are the radii of fiber cores and cladding, respectively, and n_2, n_1, and n_0 are the refractive indices of the cores, the cladding, and the surrounding medium, respectively. Based on the full-wave formulations, a combined method employing the BEM and the finite-element technique is used to solve the propagation characteristics of the inhomogeneous optical waveguide (fiber cores and cladding regions) embedded in the homogeneous surrounding medium with a dumbbell-shaped cross section [11]. In the homogeneous region with the boundary Γ, the transverse magnetic field F (= H_x or H_y) and its normal derivative dF/dn (= dH_x/dn or dH_y/dn) on Γ can be related through an integral equation

$$\frac{1}{2}F(\vec{r}) = P\int_\Gamma F(\vec{r}')\,\frac{dG(k_d,\vec{r},\vec{r}')}{dn}\,d\vec{r}' - \oint_\Gamma G(k_d,\vec{r},\vec{r}')\,\frac{dF(\vec{r}')}{dn}\,d\vec{r}' \quad (2)$$

where k_d is related to the wave number in free space k_0 and the propagation constant of the guided mode β by $k_d = (\beta^2 - k_0^2\epsilon_d)^{1/2}$ with the relative permittivity $\epsilon_d = n_0^2$, $\vec{r}$ and $\vec{r}'$ are the position vectors in the 2-D vector space with $\vec{r}'$ on Γ as shown in Fig. 2, $G = (1/2\pi)K_0(k_d|\vec{r} - \vec{r}'|)$ with K_0 being the modified Bessel function of the second kind and order zero denotes the 2-D Green function in the homogeneous cladding, and $P\int$ denotes the Cauchy principle value integral with the singularity at the point of $\vec{r} = \vec{r}'$ being removed. Through the integral equation (2), the transverse magnetic field at an arbitrary position $\vec{r}$ in surrounding medium can be described by the field on Γ and its normal derivative along $\hat{n}$. When $F(\vec{r})$ is chosen as the field on the boundary Γ, a complete relation between F and dF/dn on Γ for the surrounding homogeneous region is established in (2).

In the inhomogeneous region with the relative permittivity distribution

$$\epsilon_c(x,y) = \begin{cases} n_2^2 & \text{for the cores region} \\ n_1^2 & \text{for the cladding region} \end{cases}$$

the magnetic fields of the guided modes satisfy the following source-free equation:

$$k_0^2\vec{H} - \nabla\times\left(\frac{1}{\epsilon_c^2}\,\nabla\times\vec{H}\right) = 0. \quad (3)$$

By making the dot product of the left-hand side of (3) with an arbitrary vector function $\vec{H}^c$, which is independent of $\vec{H}$, and integrating the scalar product over the entire space, the differential equation (3) can be transformed into the variational-equation formulations. After some manipulations as shown in [11], the variational equations with the arbitrary fields $\vec{H}^c$ being chosen as $H_x^c\hat{x}$ and $H_y^c\hat{y}$, respectively, are

$$\int (k_0^2\epsilon_c - \beta^2)H_xH_x^c - \frac{\partial H_x}{\partial x}\frac{\partial H_x^c}{\partial x} - \frac{\partial H_x}{\partial y}\frac{\partial H_x^c}{\partial y} + \left(\frac{\partial H_y}{\partial x} - \frac{\partial H_x}{\partial y}\right)\frac{\partial\epsilon_c}{\partial y}\,\frac{1}{\epsilon_c}\,H_x^c\,dx\,dy = 0 \quad (4a)$$

and

$$\int (k_0^2\epsilon_c - \beta^2)H_yH_y^c - \frac{\partial H_y}{\partial x}\frac{\partial H_y^c}{\partial x} - \frac{\partial H_y}{\partial y}\frac{\partial H_y^c}{\partial y} + \left(\frac{\partial H_x}{\partial y} - \frac{\partial H_y}{\partial x}\right)\frac{\partial\epsilon_c}{\partial x}\,\frac{1}{\epsilon_c}\,H_y^c\,dx\,dy = 0. \quad (4b)$$

By making a variation of (4a) and (4b) with respect to H_x^c and H_y^c, one obtains the differential equation of H_x and H_y in (3). For guided modes, the boundary condition that E_z and H_z are continuous at the boundary Γ should be satisfied. From the

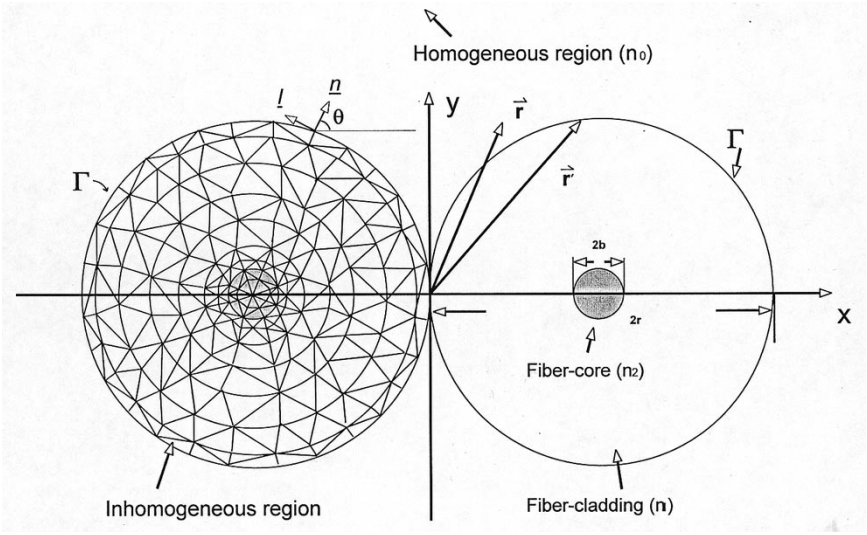

Fig. 2. Coordinate system in the combining approach employing FEM and BEM. The FEM with triangular meshes is used in the homogeneous region, which include the fiber-cores and fiber-cladding, and the BEM is applied to the homogeneous region with boundary Γ.

Maxwell equations $j\omega\epsilon\vec{E} = \nabla \times \vec{H}$ and $\nabla \cdot \vec{H} = 0$, E_z and H_z can be expressed as

$$j\omega E_z = \frac{1}{\epsilon}\left(\frac{\partial H_n}{\partial \ell} - \frac{\partial H_\ell}{\partial n}\right) \tag{5a}$$

and

$$j\beta H_z = \frac{\partial H_n}{\partial n} + \frac{\partial H_\ell}{\partial \ell} \tag{5b}$$

where $\epsilon = \epsilon_0\epsilon_c$ or $\epsilon = \epsilon_0\epsilon_d$ with ϵ_0 being the permittivity of the vacuum, H_n and H_ℓ are the magnetic fields normal to and tangential to the boundary, respectively, and $\partial/\partial n$ and $\partial/\partial \ell$ denote the partial derivatives along the normal and the tangential directions, respectively. Explicitly, $H_n = H_x\cos(\theta) + H_y\sin(\theta)$ and $H_l = H_x\sin(\theta) - H_y\cos(\theta)$, where θ is the angle between $\hat{n}$ and the x direction. Since the cross section of the weakly fused coupler possesses symmetry about y axis, only half of the inhomogeneous region is divided into triangular elements, as shown in Fig. 2, for the FEM treatment in (4). Within each element the unknown fields (H_x and H_y) and the arbitrary fields (H_x^c and H_y^c) are expanded in linear local basis functions with the expansion coefficients being the field nodal values. By taking the variation on the arbitrary fields and some matrix manipulations for (4a) and (4b), the normal derivative fields ($\partial H_x/\partial n$ and $\partial H_y/\partial n$) on the boundary Γ of the inhomogeneous region can be expressed explicitly in terms of the boundary fields (H_x and H_y). Based on the BEM with pulse bases for (2), the relations in matrix form between the normal derivative fields (dF/dn) and the boundary fields (F) on Γ of the homogeneous region can be obtained. The tangential derivative fields ($\partial H_x/\partial \ell$ and $\partial H_y/\partial \ell$) in (5) are approximated by a three-point finite difference. Through matching the continuity of E_z and H_z, respectively, in (5a) and (5b) which are now in terms of H_x and H_y only, the propagation characteristics of the guided normal modes can be obtained.

In our 3-D modeling the exponential taper profile with a waist of uniform dimension, as shown in Fig. 1, is used [1], [5]. Such taper profile of the coupler can be expressed in terms of fiber radius $r(z)$ as

$$r(z) = \begin{cases} r_0 e^{-(L/(L_b))} & |z| \le L_b/2 \\ r_0 e^{[-(L+L_b-2|z|)/(2L_b)]} & L_b/2 < |z| < (L+L_b)/2 \\ r_0 & |z| > (L+L_b)/2 \end{cases} \tag{6}$$

where r_0 is the radius of the unreduced fiber cladding, L_b is the length of the burned region, and L is the full drawn length. The radius of fiber-core $b(z)$ along the z axis is assumed to have the same functional dependence as (6). From this profile model it is clearly seen that the taper profile is determined by the burned length and the drawn length. As shown in Fig. 1, the tapered structure is divided into many small segments, which is called the step-like approximation method, and the radius of each small segment is taken as that of the middle of the segment. By accumulating the phase difference between the even and odd modes of these small segments in each polarization, we obtain $\Delta\phi_x$ and $\Delta\phi_y$, and then the power distributions at the output channels of the coupler can be determined.

III. Fiber-Cores Effect: 2-D EM Modeling

The fiber-cores effect on the propagation characteristics and mode filed patterns are investigated for the couplers in 2-D cross-section view. Rigorous mathematical analysis combining the BEM and FEM can provide the magnetic field patterns of the four normal vector modes, and the results for the weakly fused coupler with the core index profile $D \equiv (n_2^2 - n_1^2)/2n_2^2 = 0.5\%$ and the normalized frequency $V \equiv (2\pi r/\lambda)\sqrt{n_1^2 - n_0^2} = 30$ are given in Fig. 3. Fig. 3(a) and (b) shows the even mode and odd mode, respectively, with the polarization being predominantly in the x direction. Fig. 3(c) and (d) shows the corresponding modes for the y polarization. Note that magnetic fields are plotted here, although the polarization direction is defined by the electric field. Each arrow represents the orientation and the relative strength of the magnetic field at the point specified by the arrow root. Since

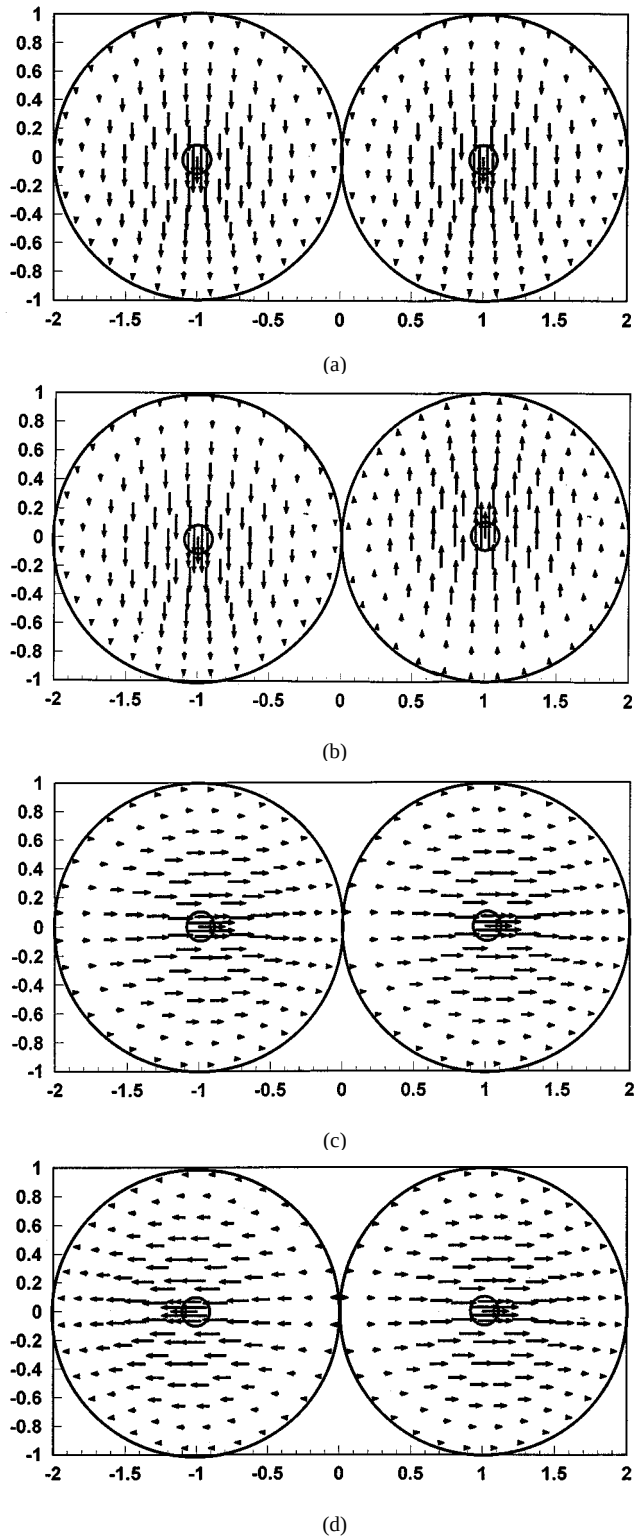

(a) (b) (c) (d)

Fig. 3. Four orthogonal vectorial mode patterns shown by the magnetic fields for the weakly fused coupler with concerning the fiber-cores. (a) Even mode with x polarization, (b) odd mode with x polarization, (c) even mode with y polarization, and (d) odd mode with y polarization.

the fused coupler, in general, is a strongly guiding waveguide, the mode fields are almost guided in the coupler. It can be found that the fiber-cores cause the concentration of power density within the core regions.

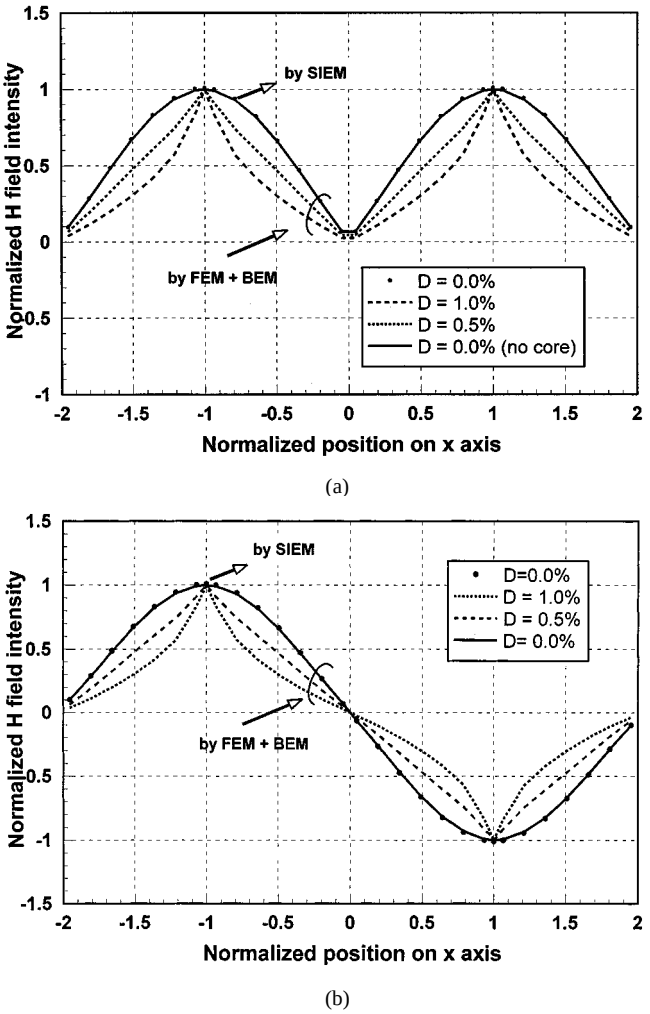

Fig. 4. Fiber-cores effects on the field distributions along the x axis. (a) Even mode and (b) odd mode. The calculated results by both the surface integral equation method (SIEM) and the combining approach (FEM and BEM) are shown and compared for the coupler with $D = 0.0\%$.

To see more clearly the fiber-core effects on the mode fields, the normalized magnetic fields in their predominant direction along the center line $(y = 0)$ of the coupler is plotted in Fig. 4 with different core index profiles ($D = 0.0\%$, $D = 0.5\%$, and $D = 1.0\%$) at $V = 30$. Fig. 4(a) and (b) show the field distributions of the even and odd modes, respectively, for the x polarization with $V = 30$. It can be seen that small perturbations of the refractive index of fiber cores from $D = 0.0\%$ (no-core approximation) to $D = 0.5\%$ or from $D = 0.5\%$ to $D = 1.0\%$ cause significant variations on the mode field distributions. To check the correctness of our combining numerical approach, we compare the calculated field distributions for $D = 0.0\%$ with the results obtained by the surface integral equation method (SIEM). The SIEM is a vectorial numerical approach that can rigorously solve the propagation characteristics of the embedded homogeneous optical waveguide with arbitrary cross-sectional shape. It is clearly presented that the field distributions obtained by these two different numerical approaches are quite consistent for the coupler without considering the fiber cores.

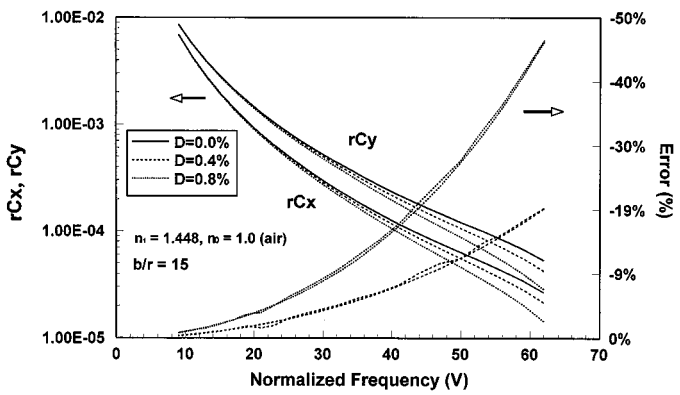

Fig. 5. Normalized coupling coefficients of y polarization rC_y as a function of V for three different core index profiles $D = 0.0\%$, $D = 0.4\%$, and $D = 0.8\%$. The percentage errors of rCy caused by neglecting the cores are also shown.

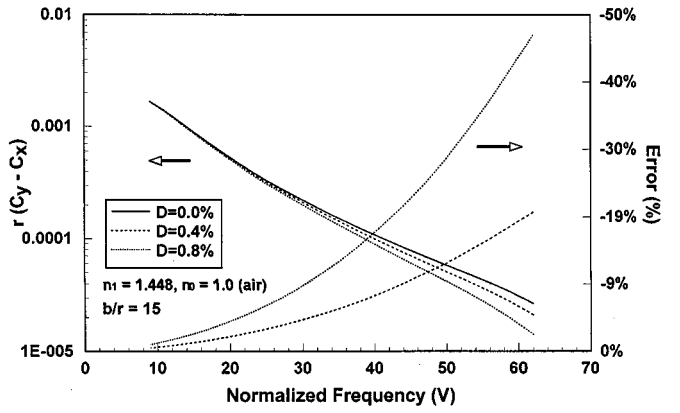

Fig. 6. Form birefringence as a function of V for three different core index profiles $D = 0.0\%$, $D = 0.4\%$, and $D = 0.8\%$. The percentage errors by neglecting the cores are also shown.

Fig. 5 shows the normalized coupling coefficients of two polarization states (rC_x and rC_y) as a function of V for three different core index profiles $D = 0.0\%$, $D = 0.4\%$, and $D = 0.8\%$ with $n_1 = 1.448$, $n_0 = 1.0$, and $r/b = 15$. The percentage error for rC_x and rC_y caused by neglecting the cores is also shown in Fig. 5. The influence of fiber cores on the coupling coefficient becomes more significant as the V-values increase. Obviously the no-core assumption can be justified only at very low V-values, which are not the cases for real couplers. Since the coupling coefficients decrease exponentially with normalized frequencies and become small at high V-values, small perturbations of fiber-cores in the couplers cause significant variations of the coupling strength. It can be seen that the percentage error of rC_x or rC_y can reach about 19% and 45% for the perturbations of the refractive index of the fiber-cores with $D = 0.4\%$ and $D = 0.8\%$, respectively, at normalized frequency $V = 60$. The fiber-core effect on the form birefringence, which is defined as $r(C_y - C_x)$, is illustrated in Fig. 6 with the coupler parameters being the same as in Fig. 5. The percentage error for the birefringence by ignoring the cores also becomes significant as V increases. The error can reach about 50% and 20% for $D = 0.4\%$ and $D = 0.8\%$, respectively, at the normalized frequency $V = 60$. Because the error behaviors, as shown in Fig. 5, for the two polarization states are similar, it is reasonable to see that the behavior of birefringence error by neglecting the fiber-cores is quite similar to the error behavior of coupling coefficients.

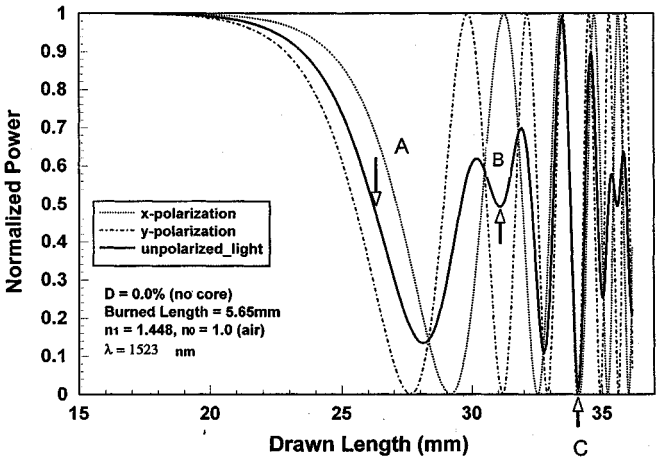

Fig. 7. Normalized output power (P_1/P_0) variation of a practical weakly fused tapered coupler in the drawing process for the input light with three different types of polarization property. A 3-dB power divider, PBS, and WDMC can be obtained by stopping at point A, B, and C, respectively.

IV. Fiber-Cores Effect: 3-D EM Modeling

As described in (1), the coupling behavior of the fused tapered couplers is determined by the accumulated phase difference between the coupling modes along the coupling region with varying V-values. Although it has been presented in previous section that the fiber-cores effects on the coupling coefficients and the birefringence are significant for large V-values, the performance of the real coupler is not easy to be predicted by just knowing the coupling characteristics at the cross section of the coupler. Based on the rigorous numerical approach as described in Section II, the influence of the fiber-cores on the modeling of the coupling behaviors for the couplers, such as power divider, polarization beam-splitter (PBS), and wavelength demultiplexing/multiplexing coupler (WDMC), is investigated in this section.

Fig. 7 shows the normalized output power (P_1/P_0) variation of a practical weakly fused tapered coupler in the drawing process for the input light with three different types of polarization property, x-polarization ($P_{0y} = 0$), y-polarization ($P_{0x} = 0$), and unpolarization ($P_{0x} = P_{0y}$). The standard telecommunication fibers with $2b = 9$ μm and $2r = 125$ μm are used, and the input light wavelength is 1523-nm. The burned length L_b for the exponential taper profile is 5.65 mm and the fiber cores are neglected. The intensity of the output power cyclically reaches 100% for the input light with x and y polarization states as the fibers are pulled. The coupling patterns for these two polarization states are similar, but coupling occurs first for the y polarization because C_y is larger than C_x for the couplers in weakly fused conditions. Due to the form birefringence of the weakly fused coupler, the polarization modulation envelope of the normalized output power is clearly seen for the case with the unpolarized input light. A 3 dB power divider, PBS, and WDMC can be obtained by stopping at the drawn length of 26.2, 31.2,

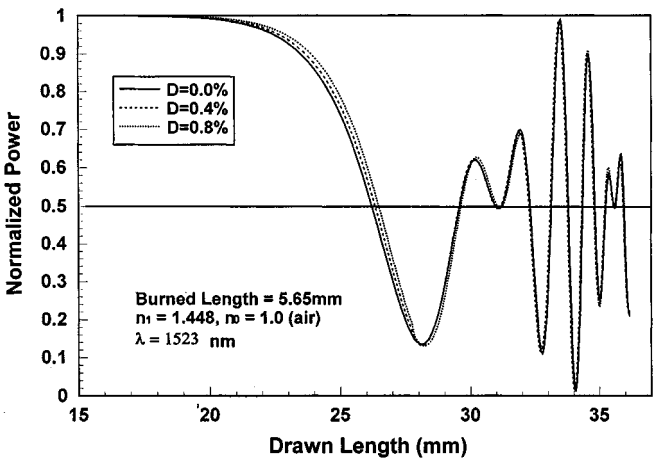

Fig. 8. Cores effect on the normalized output power in the drawing process with $D = 0.0\%$, $D = 0.4\%$, and $D = 0.8\%$.

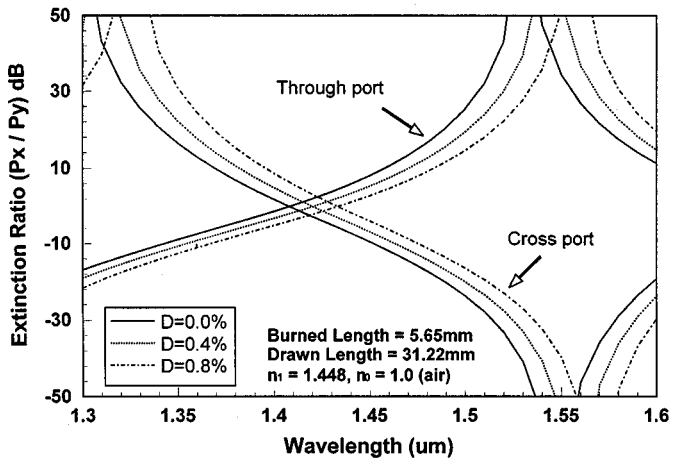

Fig. 10. The influence of the fiber cores on the wavelength responses of the extinction ratio for a PBS with $L_b = 5.65$ mm and $L = 31.22$ mm.

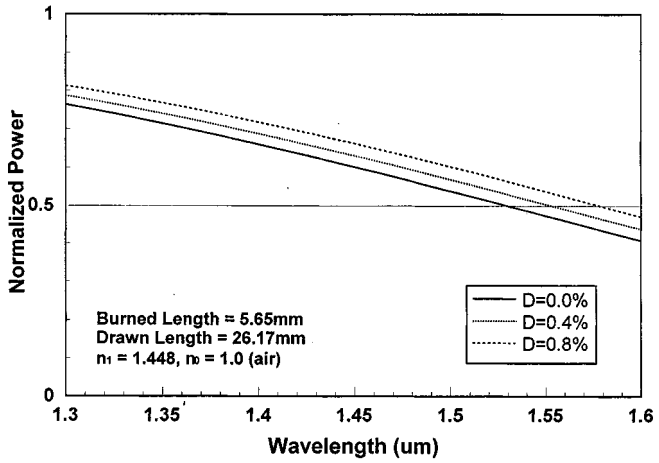

Fig. 9. The influence of fiber-cores on the wavelength responses of the normalized output power at through port for a 3 dB coupler.

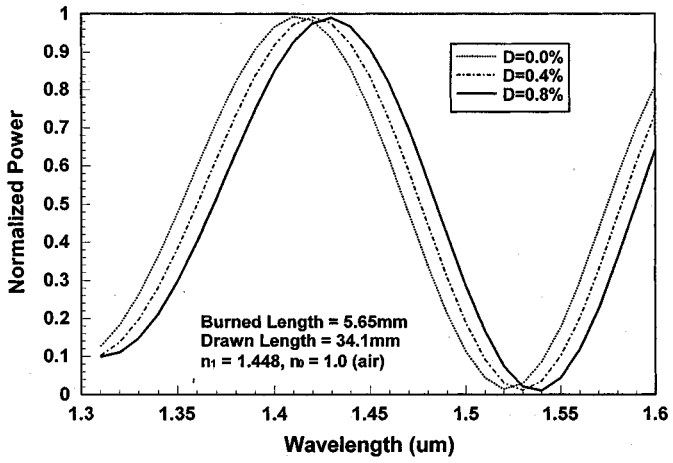

Fig. 11. Fiber-cores effect on the spectral responses of the normalized output power at the through port for a WDMC with $L_b = 5.65$ mm and $L = 34.1$ mm.

and 34.2 mm as indicated by point A, B, and C, respectively, in Fig. 7. At point A, the unpolarized input power is equally distributed between the two output ports. At point B the coupling ratio at through port is 100% for the input light with x polarization and 0% for that with y polarization [4] and [12]. At point C the coupled power at the through port for the unpolarized input light with 1523-nm wavelength is relative minimum [13].

Fig. 8 shows the cores effect on the normalized output power in the drawing process with $D = 0.0\%$, $D = 0.4\%$, and $D = 0.8\%$. When the coupler has shorter drawn length, the V-value at the coupler waist is larger and thus the effect of fiber cores can be seen. However, when the coupler has longer elongation, the difference in the coupling behavior between the real couplers ($D = 0.4\%$ and $D = 0.8\%$) and the no-core coupler ($D = 0.0\%$) is small because of the smaller V-value at the coupler waist.

Fig. 9 shows the fiber cores effect on the wavelength responses of the normalized output power at through port for a 3-dB coupler with $L_b = 5.65$ mm and $L = 26.17$ mm. The output power decreases almost linearly with wavelength for both real couplers ($D = 0.4\%$ and $D = 0.8\%$) and no-core coupler ($D = 0.0\%$), but the wavelength for 50% coupling ratio increases with the refractive index profiles of cores being increased. It is seen that the discrepancy for the coupler's performance is significant between the real coupler and the no-core coupler. Fig. 10 shows the influence of the fiber cores on the wavelength responses of the extinction ratio, which is defined as the P_y/P_x (where P_y and P_x are the output powers at the port considered for x and y polarizations), for a PBS with $L_b = 5.65$ mm and $L = 31.22$ mm. If a PBS is theoretically assumed as the coupler with the extinction ratio being larger than 50 dB at both output ports, it can be seen that the couplers with $D = 0.0\%$, $D = 0.4\%$, and $D = 0.8\%$ perform as PBS's at wavelength of 1540 nm, 1550 nm, and 1560 nm, respectively. Therefore, the accuracy of predicting the performance of the real fused coupler by neglecting the fiber cores is not valid in the 3-D EM modeling, although the trend of the coupling behavior of the real couplers can be modeled by the couplers with no-core assumption. Fig. 11 shows the spectral responses of the normalized output power at the through port for a WDMC with $L_b = 5.65$ mm and $L = 34.1$ mm. Again, there are significant discrepancies for the wavelength responses between

real couplers with $D = 0.4\%$ and $D = 0.8\%$ and the no-core coupler. It can be found that the real couplers with $D = 0.4\%$ and $D = 0.8\%$ perform as WDMC's at the wavelegths 1420 nm/1530 nm and 1430 nm/1540 nm, respectively, but it occurs at wavelengths 1410 nm/1520 nm for the coupler with no-core assumption.

It is worth noting that although the cores effects on the coupling characteristics, as shown in Section III, is quite significant at high V-values in 2-D view, their effects on the coupling behavior for the realistic couplers is not so dramatic. It can be explained as the small V-value at the waist region of the weakly fused coupler. In our 3-D modeling, the transverse dimension of the weakly fused coupler is reduced exponentially in the tapered region and keeps uniform at the waist region with the length being the burned length L_b. Therefore, the coupling behavior of the real coupler is dominantly decided by the coupling characteristics in the waist region because the coupling strength in this region is the strongest due to the smallest V-value. It can be found that the normalized frequency V at the waist is about 26, 17, and 12 for the power divider, PBS, and WDMC, respectively, in previous study. As shown in Section III, the errors of the coupling characteristics by neglecting the fiber cores are relatively small at these small V-values.

V. Conclusion

Based on the vectorial electromagnetic formulations, which combines the finite element method and the boundary element technique, and the step-like approximation method, a 3-D electromagnetic modeling program has been established to study the fiber cores effects on the coupling characteristics of the weakly fused tapered couplers both in 2-D and 3-D EM views. It has been found that the cores have significant effect on the mode field distributions and the errors of the coupling coefficients and the birefringence by neglecting the cores increases dramatically as V-values increases. The influence of the fiber cores on the coupling behavior for the practical couplers, such as 3 dB power divider, PBS, and WDMC, have also been studied in this paper. We have found that the model with no-core assumption can only predict the trend of the coupling behavior for the real coupler, but the discrepancies of the coupler's performance can be significant between the real couplers and no-core couplers. The effects of fiber-cores in the weakly fused tapered couplers have to be considered for more accurately modeling their coupling characteristics.

References

[1] M. Eisenmann and E. Weidel, "Single-mode fused biconical couplers for wavelength division multiplexing with channel spacing between 100 and 300 nm," *J. Lightwave Technol.*, vol. 6, pp. 113–119, 1988.

[2] S. Lacroix, F. Gonthier, and J. Bures, "Modeling of symmetric 2×2 fused-fiber couplers," *Appl. Opt.*, vol. 33, pp. 8361–8369, 1994.

[3] K. Okamoto, "Theoretical investigation of light coupling phenomena in wavelength-flattened couplers," *J. Lightwave Technol.*, vol. 8, pp. 678–683, 1990.

[4] I. Yokohama, K. Okamoto, and J. Noda, "Analysis of fiber-optic polarizing beam splitters consisting of fused-taper couplers," *J. Lightwave Technol.*, vol. 4, pp. 1352–1359, 1986.

[5] S. W. Yang, T. L. Wu, and H. C. Chang, "Numerical modeling of weakly fused fiber-optic polarization beamsplitters—Part II: The three-dimensional electromagnetic model," *J. Lightwave Technol.*, vol. 16, pp. 691–696, 1998.

[6] X. H. Zheng, "Finite-element analysis of fused couplers," *Electron. Lett.*, vol. 22, pp. 623–625, 1986.

[7] T. L. Wu and H. C. Chang, "Rigorous analysis of form birefringence of weakly fused fiber-optic couplers," *J. Lightwave Technol.*, vol. 13, pp. 687–691, 1995.

[8] C. C. Su, "A surface equation method for homogeneous optical fibers and coupled image lines of arbitrary cross section," *IEEE Trans. Microwave Theory Tech.*, vol. MTT-33, pp. 1114–1120, 1985.

[9] M. N. McLandrich, "Core dopant profiles in weakly fused single-mode fibers," *Electron. Lett.*, vol. 24, pp. 1654–1656, 1991.

[10] K. S. Ching, "Analysis of fused couplers by the effective-index method," *Electron. Lett.*, vol. 22, pp. 1221–1222, 1986.

[11] C.-C. Su, "A combined method for dielectric waveguides using the finite-element technique and the surface integral equations method," *IEEE Trans. Microwave Theory Tech.*, vol. MTT-34, pp. 1140–1146, 1986.

[12] C. W. Wu, T. L. Wu, and H. C. Chang, "A novel fabrication method for all-fiber, weakly fused, polarization beamsplitters," *IEEE Photon. Technol. Lett.*, vol. 7, pp. 786–788.

[13] M. M. McLandrich, R. J. Orazi, and H. R. Marlin, "Polarization independent narrow channel wavelength division multiplexing fiber couplers for 1.55 μm," *J. Lightwave Technol.*, vol. 9, pp. 442–447, 1991.

Tzong-Lin Wu (M'98) was born in Hsinchu, Taiwan, R.O.C., on June 23,1969. He received the B.S.E.E. and Ph.D. degrees from National Taiwan University, Taipei, Taiwan, in 1991 and 1995, respectively.

From 1995 to 1996, he was a Senior Engineer at the Microelectronics Technology, Inc., Hsinchu, Taiwan, a wireless/satellite communications company dedicated to the development of RF modules. From 1996 to 1998, he joined the Central Research Institute, Tatung Company, Taipei, Taiwan, where he was involved with the analysis and measurement of EMC/EMI problems of high-speed digital systems. In August 1998,he joined the faculty of Electrical Engineering Department of National Sun Yat-Sen University, where he is currently an assistant professor. His research interests include design and analysis of fiber-optic components, EMC for high-speed digital systems, and RF circuits design.